Computational Geosciences **6:** 315–332, 2002.

Enhanced velocity mixed finite element methods for flow in multiblock domains

John A. Wheeler [a], Mary F. Wheeler [b] and Ivan Yotov [c]

[a] *Texas Institute for Computational and Applied Mathematics (TICAM), The University of Texas at Austin, Austin, TX 78712, USA*
E-mail: jwheeler@ticam.utexas.edu

[b] *TICAM, Department of Aerospace Engineering & Engineering Mechanics, and Department of Petroleum and Geosystems Engineering, The University of Texas at Austin, Austin, TX 78712, USA*
E-mail: mfw@ticam.utexas.edu

[c] *Department of Mathematics, University of Pittsburgh, Pittsburgh, PA 15260, USA*
E-mail: yotov@math.pitt.edu

Received 5 August 2001; accepted 15 January 2002

The paper presents a new approach to discretizing flow in porous media via mixed finite element methods on non-matching multiblock grids. The velocity space along the interfaces is enhanced to give flux-continuous approximation. No additional matching conditions need to be imposed. The computational complexity of the resulting algebraic problem is comparable to the one for the single-block case. A priori error estimates for the pressure and the velocity and numerical experiments confirming the theory are presented.

Keywords: mixed finite element methods, non-matching grids, porous media

1. Introduction

We consider mixed finite element methods for flow in multiblock domains. Mixed methods are especially useful for porous media problems due to their local mass conservation and explicit approximation of the velocity vector. In a multiblock formulation the domain is decomposed into a series of subdomains (blocks). The equations hold with their usual meaning on the subdomains, with physically meaningful boundary conditions imposed on the interfaces. Each block is independently covered by a local grid. The grids do not have to match on interfaces between blocks. This approach allows for efficient couplings of different physical and numerical models, flexible gridding of irregular geometries, and proper treatment of internal boundaries such as faults, layers, and discontinuous coefficients.

Mortar mixed finite element methods have been successfully used to handle non-matching grids in the multiblock framework [2,7,25]. A non-mortar approach based on Robin interface conditions has also been developed [5]. Both methods lead to non-

conforming discretizations with flux-matching imposed weakly through Lagrange multipliers. The reader is referred to [6,8,13,24] and references therein for the use of mortars in the context of Galerkin finite element and finite volume methods.

In this paper we study an alternative approach based on enhancing the velocity space along the subdomain interfaces. This allows for constructing flux-continuous velocity approximation. The advantage of this formulation is that, unlike the mortar method, no interface problem has to be solved, which eliminates one of the nested iterative loops. The complexity of the resulting algebraic problem is comparable to the one for the single-block case.

The enhanced velocity formulation has been implemented in the three-dimensional multiblock multiphysics parallel simulator IPARS [22,23] for modeling multiphase flow, developed at the University of Texas at Austin Center for Subsurface Modeling. The method has been tested for modeling single-phase flow, two-phase flow, and three-phase (Black Oil) flow. The mortar formulation is also implemented in IPARS, allowing for direct comparison of the accuracy and efficiency of the two methods. Our numerical experiments (see section 5) indicate that the enhanced velocity scheme is an order of magnitude faster than the current implementation of the mortar method, while providing similar accuracy.

The IPARS implementation is based on the lowest order Raviart–Thomas mixed finite element spaces RT_0 [17,18,21]. It reduces the mixed method to cell-centered finite differences for pressures (and, for multiphase flow, saturations) via application of appropriate quadrature rules which allow the velocities to be eliminated [4,20]. In this context the enhanced velocity method can be viewed as an extension to non-matching grids of known cell-centered finite difference methods on locally refined grids [12,14].

The rest of the paper is organized as follows. In the next section the method is formulated for single-phase flow. A priori error estimates for the pressure and the velocity are derived in section 3. In section 4, an extension of the method to two-phase flow is given. Implementation details and numerical results are presented in section 5. The paper ends with conclusions in section 6.

2. Formulation of the method for single-phase flow

We consider the following single-phase flow model for the pressure p and the velocity $\mathbf{u}$:

$$\mathbf{u} = -K\nabla p \quad \text{in } \Omega, \tag{2.1}$$

$$\nabla \cdot \mathbf{u} = f \quad \text{in } \Omega, \tag{2.2}$$

$$p = g \quad \text{on } \partial\Omega, \tag{2.3}$$

where $\Omega = \bigcup_{i=1}^{n} \Omega_i \subset \mathbb{R}^d$, $d = 2$ or 3, is a multiblock domain and K is a symmetric, uniformly positive definite tensor representing the permeability divided by the viscosity. The Dirichlet boundary conditions are considered merely for simplicity. For clarity of the presentation we also assume that the problem is H^2-regular (see [16] for sufficient

conditions). The subdomains Ω_i are assumed to be non-overlapping. We let $\Gamma_{i,j} = \partial\Omega_i \cap \partial\Omega_j$, $\Gamma = \bigcup_{i,j=1}^{n} \Gamma_{i,j}$, and $\Gamma_i = \partial\Omega_i \cap \Gamma = \partial\Omega_i \backslash \partial\Omega$ denote interior block interfaces. The functional spaces for the mixed weak formulation of (2.1)–(2.3) are defined as usual [9] to be

$$\mathbf{V} = H(\mathrm{div};\Omega) = \left\{\mathbf{v} \in \left(L^2(\Omega)\right)^d \colon \nabla\cdot\mathbf{v} \in L^2(\Omega)\right\},$$
$$W = L^2(\Omega).$$

We will make use of the following standard notation. For a subdomain $G \subset \mathbb{R}^d$, the $L^2(G)$ inner product (or duality pairing) and norm are denoted $(\cdot,\cdot)_G$ and $\|\cdot\|_G$, respectively, for scalar and vector valued functions. The Sobolev spaces $W_p^k(G)$, $k \in \mathbb{R}$, $1 \leqslant p \leqslant \infty$, are defined in the usual ways [1] with the usual norm $\|\cdot\|_{k,p,G}$. Let $\|\cdot\|_{k,G}$ be the norm of the Hilbert space $H^k(G) = W_2^k(G)$. We omit G in the subscript if $G = \Omega$. For a section of a subdomain boundary $S \subset \bigcup_{i=1}^{n} \partial\Omega_i$ we write $\langle\cdot,\cdot\rangle_S$ and $\|\cdot\|_S$ for the $L^2(S)$ inner product (or duality pairing) and norm, respectively.

With the above notation we have

$$\|\mathbf{v}\|_{\mathbf{V}} = \left(\|\mathbf{v}\|^2 + \|\nabla\cdot\mathbf{v}\|^2\right)^{1/2}, \qquad \|w\|_W = \|w\|.$$

A weak solution of (2.1)–(2.3) is a pair $\mathbf{u} \in \mathbf{V}$, $p \in W$ such that

$$\left(K^{-1}\mathbf{u}, \mathbf{v}\right) = (p, \nabla\cdot\mathbf{v}) - \langle g, \mathbf{v}\cdot\nu\rangle_{\partial\Omega}, \quad \mathbf{v} \in \mathbf{V}, \tag{2.4}$$
$$(\nabla\cdot\mathbf{u}, w) = (f, w), \qquad w \in W. \tag{2.5}$$

It is well known (see, e.g., [9,19]) that (2.4), (2.5) have a unique solution.

We next present the finite element discretization of (2.4), (2.5). Although the method can be defined for all of the usual mixed finite element spaces on simplicial and rectangular-type elements (see [9]), for simplicity of the presentation we restrict our discussion to the most commonly used Raviart–Thomas spaces of lowest order RT_0 [17,18,21] on rectangles (if $d = 2$) or bricks (if $d = 3$).

Let $\mathcal{T}_{h,i}$ be a rectangular partition of Ω_i, $1 \leqslant i \leqslant n$. The subdomain partitions $\mathcal{T}_{h,i}$ and $\mathcal{T}_{h,j}$ need not match on $\Gamma_{i,j}$. Let $\mathcal{T}_h = \bigcup_{i=1}^{n} \mathcal{T}_{h,i}$. The RT_0 spaces are defined for any element $E \in \mathcal{T}_h$ as follows:

$$\mathbf{V}_h(E) = \left\{\mathbf{v} = (v_1, v_2) \text{ or } \mathbf{v} = (v_1, v_2, v_3) \colon v_l = \alpha_l + \beta_l x_l;\ \alpha_l, \beta_l \in \mathbb{R},\ l = 1, \ldots, d\right\},$$
$$W_h(E) = \{w = \text{const}\}.$$

The degrees of freedom for a vector $\mathbf{v} \in \mathbf{V}_h(E)$ can be specified by the values of its normal components $\mathbf{v}\cdot\nu$ at the midpoints of all edges (faces) of E, where ν is the outward unit normal vector on ∂E. The degree of freedom for a function $w \in W_h(E)$ is its value at the center of E (see figure 1).

The pressure finite element space on Ω is defined in the usual way:

$$W_h = \left\{w \in L^2(\Omega) \colon w|_E \in W_h(E),\ \forall E \in \mathcal{T}_h\right\}.$$

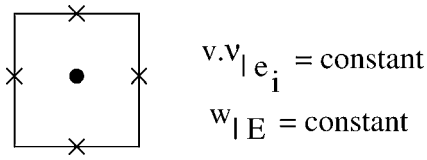

Figure 1. Degrees of freedom for the lowest order Raviart–Thomas spaces.

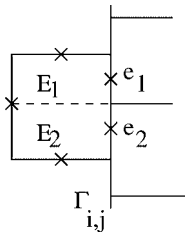

Figure 2. Degrees of freedom for the enhanced velocity space.

Note that, since W_h is a discontinuous space, no special care is needed on the interfaces. Our goal is to construct a velocity finite element space $V_h^* \subset V$ on the multiblock partition $\mathcal{T}_h$ of Ω. Let, for $i = 1, \ldots, n$,

$$\mathbf{V}_{h,i} = \big\{\mathbf{v} \in H(\mathrm{div};\, \Omega_i)\colon\ \mathbf{v}|_E \in \mathbf{V}_h(E),\ \forall E \in \mathcal{T}_{h,i}\big\},$$

be the usual RT_0 velocity space on Ω_i. The product space

$$\mathbf{V}_h = \mathbf{V}_{h,1} \oplus \mathbf{V}_{h,2} \oplus \cdots \oplus \mathbf{V}_{h,n}$$

however is not a subspace of $H(\mathrm{div};\, \Omega)$ since the normal vector components do not match on Γ. We thus need to modify the degrees of freedom on Γ. Let $\mathcal{T}_{h,i,j}$ be the rectangular partition of $\Gamma_{i,j}$ obtained from the intersection of the traces of $\mathcal{T}_{h,i}$ and $\mathcal{T}_{h,j}$. (We assume that in 3D the subdomains do not meet at an angle.) We force the fluxes to match on each element $e \in \mathcal{T}_{h,i,j}$. Consider any element $E \in \mathcal{T}_{h,i}$ such that $E \cap \Gamma_{i,j} \neq \emptyset$. The interface grid may divide the boundary edge (face) of E into several parts. This division can be extended inside the element as shown in figure 2. On each subelement E_k we define a basis function $\mathbf{v}_{E_k}$ in the RT_0 space $\mathbf{V}_h(E_k)$ which has a normal component $\mathbf{v}_{E_k} \cdot \nu$ equal to one on e_k and zero on the other edges (faces). Let $\mathbf{V}_h^\Gamma$ be the span of all such basis functions. We define the multiblock mixed finite element velocity space to be

$$\mathbf{V}_h^* = \big(\mathbf{V}_{h,1}^0 \oplus \mathbf{V}_{h,2}^0 \oplus \cdots \oplus \mathbf{V}_{h,n}^0 \oplus \mathbf{V}_h^\Gamma\big) \cap H(\mathrm{div};\, \Omega),$$

where $\mathbf{V}_{h,i}^0$ is the subspace of $\mathbf{V}_{h,i}$ with zero normal trace on Γ_i. We call $\mathbf{V}_h^*$ an enhanced velocity space. The addition of the interface degrees of freedom allows for imposing flux continuity on the finer interface grid $\mathcal{T}_h^\Gamma = \bigcup_{1 \leqslant i \leqslant j} \mathcal{T}_{h,i,j}$ and thus constructing an

$H(\mathrm{div};\Omega)$ – conforming velocity approximation. The price to pay is that this definition modifies the usual RT_0 velocity space on all elements neighboring Γ (see figure 2), which leads to some difficulties in the analysis of the method.

With the above defined spaces we have the following mixed finite element discretization of (2.4), (2.5): find $\mathbf{u}_h \in \mathbf{V}_h^*$ and $p_h \in W_h$ such that

$$\left(K^{-1}\mathbf{u}_h, \mathbf{v}\right) = (p_h, \nabla\cdot\mathbf{v}) - \langle g, \mathbf{v}\cdot\nu\rangle_{\partial\Omega}, \quad \mathbf{v}\in\mathbf{V}_h^*, \tag{2.6}$$

$$(\nabla\cdot\mathbf{u}_h, w) = (f, w), \quad w\in W_h. \tag{2.7}$$

3. Analysis of the single-phase flow model

One possible approach to analyzing (2.6), (2.7) is to employ the general saddle-point problem theory (see, e.g., [9,15]). It is easy to check that the inf–sup condition

$$\inf_{w\in W_h\setminus\{0\}} \sup_{v\in\mathbf{V}_h^*\setminus\{0\}} \frac{(\nabla\cdot\mathbf{v}, w)}{\|\mathbf{v}\|_{\mathbf{V}}\|w\|_W} \geqslant \beta \tag{3.1}$$

holds for the pair $(\mathbf{V}_h^*, W_h)$ with a constant $\beta > 0$ independent of h. The main tool for proving (3.1) is the construction of a projection operator Π^* from $H^1(\Omega)$ onto $\mathbf{V}_h^*$ defined locally for any $E\in\mathcal{T}_h$ and any $\mathbf{q}\in H^1(E)$ as follows:

$$\int_e \left(\Pi^*\mathbf{q} - \mathbf{q}\right)\cdot\nu\,\mathrm{d}s = 0$$

where e is any edge (face) of E not lying on Γ or a part of an interface edge (face) of E which is an element of the interface grid $\mathcal{T}_h^\Gamma$. We note that an application of the divergence theorem implies that

$$\left(\nabla\cdot\left(\Pi^*\mathbf{q} - \mathbf{q}\right), w\right) = 0, \quad \forall w\in W_h. \tag{3.2}$$

Since $\mathbf{V}_h^*(E) \supset \mathbf{V}_h(E)$, the enhanced velocity space has at least as good approximation properties as the original RT_0 space and it holds that [9,18]

$$\left\|\mathbf{q} - \Pi^*\mathbf{q}\right\| \leqslant C\|\mathbf{q}\|_1 h \tag{3.3}$$

for any $\mathbf{q}\in H^1(\Omega)$. We must note however that, for $\mathbf{v}\in\mathbf{V}_h^*$, $\nabla\cdot\mathbf{v}$ may be a piecewise constant on an element E that touches Γ. Therefore

$$\nabla\cdot\mathbf{V}_h^* \supset W_h$$

but the two spaces may be different. There are two consequences of this fact. First, $\nabla\cdot\Pi^*\mathbf{q}$ does not equal the L^2-projection of $\nabla\cdot\mathbf{q}$ onto W_h; thus, no approximation properties hold for $\nabla\cdot\Pi^*\mathbf{q}$. This is in contrast to the usual mixed projection operator Π defined on the original RT_0 space $\mathbf{V}_{h,i}$ on each Ω_i [9,18], which satisfies for any $\mathbf{q}\in H^1(\Omega_i)$

$$\|\mathbf{q} - \Pi\mathbf{q}\|_{\Omega_i} \leqslant C\|\mathbf{q}\|_{1,\Omega_i} h, \tag{3.4}$$

$$\left\|\nabla\cdot(\mathbf{q} - \Pi\mathbf{q})\right\|_{\Omega_i} \leqslant C\|\nabla\cdot\mathbf{q}\|_{r,\Omega_i} h^r, \quad 0\leqslant r\leqslant 1. \tag{3.5}$$

Second, if $\mathbf{v} \in \mathbf{V}_h^*$ is a discretely divergence free vector, i.e., if $\mathbf{v} \in \mathbf{Z}_h$, where

$$\mathbf{Z}_h = \{\mathbf{v} \in \mathbf{V}_h^*\colon\ (\nabla \cdot \mathbf{v}, w) = 0\ \forall w \in W_h\},$$

then $\nabla \cdot \mathbf{v}$ may not be zero (e.g. $\nabla \cdot \mathbf{v} = 1$ on half of E and $\nabla \cdot \mathbf{v} = -1$ on the other half). Therefore the second condition needed in the general saddle-point problem theory, coercivity of $(K^{-1}\mathbf{v}, \mathbf{v})$ in $\mathbf{Z}_h$, does not hold with a constant independent of h and the theory would not yield convergence bounds.

We take a direct approach to proving solvability and convergence of (2.6), (2.7).

Lemma 3.1. There exists a unique solution of (2.6), (2.7).

Proof. Since (2.6), (2.7) is a square system, it is enough to show uniqueness. Let $f = 0$ and $g = 0$. Taking $\mathbf{v} = \mathbf{u}_h$ and $w = p_h$ leads to $\mathbf{u}_h = 0$. Therefore $(p_h, \nabla \cdot \mathbf{v}) = 0$ for all $\mathbf{v} \in \mathbf{V}_h^*$. Since $\nabla \cdot \mathbf{V}_h^* \supset W_h$, this implies that $p_h = 0$. □

In the analysis below we make use of one more projection operator. For any $\varphi \in L^2(\Omega)$, let $\hat{\varphi} \in W_h$ be its $L^2(\Omega)$ projection satisfying

$$(\varphi - \hat{\varphi}, w) = 0, \quad w \in W_h.$$

This operator has the standard L^2-projection approximation property

$$\|\varphi - \hat{\varphi}\| \leqslant C\|\varphi\|_r h^r, \quad 0 \leqslant r \leqslant 1. \tag{3.6}$$

We will also need the following bound on $\nabla \cdot \Pi^*\mathbf{q}$.

Lemma 3.2. For all $\mathbf{q} \in H^1(\Omega)$, there exists a constant C independent of h such that

$$\|\nabla \cdot \Pi^*\mathbf{q}\| \leqslant C\|\mathbf{q}\|_1. \tag{3.7}$$

Proof. Using the triangle inequality, the inverse inequality, and (3.3)–(3.5) we have

$$\begin{aligned}
\|\nabla \cdot \Pi^*\mathbf{q}\| &\leqslant \|\nabla \cdot (\Pi^*\mathbf{q} - \Pi\mathbf{q})\| + \|\nabla \cdot \Pi\mathbf{q}\| \\
&\leqslant C\big(h^{-1}\|\Pi^*\mathbf{q} - \Pi\mathbf{q}\| + \|\nabla \cdot \mathbf{q}\|\big) \\
&\leqslant C\big(h^{-1}\|\Pi^*\mathbf{q} - \mathbf{q}\| + h^{-1}\|\mathbf{q} - \Pi\mathbf{q}\| + \|\nabla \cdot \mathbf{q}\|\big) \\
&\leqslant C\|\mathbf{q}\|_1.
\end{aligned}$$

□

3.1. Velocity error estimates

To analyze the convergence properties of (2.6), (2.7) we subtract the two equations from (2.4), (2.5) to form the error equations

$$\big(K^{-1}(\mathbf{u} - \mathbf{u}_h), \mathbf{v}\big) = (p - p_h, \nabla \cdot \mathbf{v}), \quad \mathbf{v} \in \mathbf{V}_h^*, \tag{3.8}$$

$$\big(\nabla \cdot (\mathbf{u} - \mathbf{u}_h), w\big) = 0, \quad w \in W_h. \tag{3.9}$$

We first note that, using (3.2), (3.9) can be rewritten as

$$\big(\nabla\cdot\big(\Pi^*\mathbf{u}-\mathbf{u}_h\big),w\big)=0,\quad w\in W_h. \tag{3.10}$$

We now take $\mathbf{v}=\Pi^*\mathbf{u}-\mathbf{u}_h$ and $w=\hat{p}-p_h$ to get

$$\begin{aligned}&\big(K^{-1}\big(\Pi^*\mathbf{u}-\mathbf{u}_h\big),\Pi^*\mathbf{u}-\mathbf{u}_h\big)\\&\quad=\big(K^{-1}\big(\Pi^*\mathbf{u}-\mathbf{u}\big),\Pi^*\mathbf{u}-\mathbf{u}_h\big)+\big(p-\hat{p},\nabla\cdot\big(\Pi^*\mathbf{u}-\mathbf{u}_h\big)\big).\end{aligned} \tag{3.11}$$

To bound the second term on the right we note that, due to (3.10),

$$\nabla\cdot\big(\Pi^*\mathbf{u}-\mathbf{u}_h\big)\big|_E=0\quad\forall E\in\mathcal{T}_h \text{ such that } E\cap\Gamma=\emptyset.$$

Let Ω^* be the union of all $E\in\mathcal{T}_h$ such that $E\cap\Gamma\neq\emptyset$. We then have

$$\begin{aligned}\big(p-\hat{p},\nabla\cdot\big(\Pi^*\mathbf{u}-\mathbf{u}_h\big)\big)&=\big(p-\hat{p},\nabla\cdot\big(\Pi^*\mathbf{u}-\mathbf{u}_h\big)\big)_{\Omega^*}\\&\leqslant Ch\|p\|_{1,\Omega^*}h^{-1}\big\|\Pi^*\mathbf{u}-\mathbf{u}_h\big\|_{\Omega^*}\\&\leqslant Ch^{1/2}\|p\|_{1,\infty,\Omega^*}\big\|\Pi^*\mathbf{u}-\mathbf{u}_h\big\|,\end{aligned} \tag{3.12}$$

where we used (3.6) and an inverse inequality in the first inequality and that $|\Omega^*|\leqslant Ch$ in the second inequality. A combination of (3.11), (3.12), and (3.3) leads to the following result.

Theorem 3.1. For the velocity $\mathbf{u}_h$ of the mixed method (2.6), (2.7), there exists a constant C dependent on Ω and $\|K\|_{0,\infty}$ but independent of h such that

$$\|\mathbf{u}-\mathbf{u}_h\|\leqslant C\big(\|p\|_{1,\infty,\Omega^*}h^{1/2}+\|\mathbf{u}\|_{1,\Omega}h\big). \tag{3.13}$$

3.2. Pressure error estimates

We use a duality argument to derive a bound on $p-p_h$. Let φ be the solution of

$$\begin{aligned}-\nabla\cdot K\nabla\varphi&=-(\hat{p}-p_h)&&\text{in }\Omega,\\\varphi&=0&&\text{on }\partial\Omega.\end{aligned}$$

By elliptic regularity,

$$\|\varphi\|_2\leqslant C\|\hat{p}-p_h\|_0. \tag{3.14}$$

In the argument below the generic constant C may depend on $\|K\|_{1,\infty}$. Take $\mathbf{v}=\Pi^*K\nabla\varphi$ in (3.8) to get

$$\begin{aligned}\|\hat{p}-p_h\|_0^2&=\big(\hat{p}-p_h,\nabla\cdot\Pi^*K\nabla\varphi\big)\\&=\big(K^{-1}(\mathbf{u}-\mathbf{u}_h),\Pi^*K\nabla\varphi\big)+\big(\hat{p}-p,\nabla\cdot\Pi^*K\nabla\varphi\big).\end{aligned} \tag{3.15}$$

The second term on the right can be bounded as follows, using (3.6) and (3.7):

$$\big(\hat{p}-p,\nabla\cdot\Pi^*K\nabla\varphi\big)\leqslant Ch\|p\|_1\|\varphi\|_2. \tag{3.16}$$

For the first term on the right in (3.15) we write

$$\begin{aligned}\left(K^{-1}(\mathbf{u}-\mathbf{u}_h),\Pi^* K\nabla\varphi\right) &= \left(K^{-1}(\mathbf{u}-\mathbf{u}_h),\Pi^* K\nabla\varphi - K\nabla\varphi\right) + (\mathbf{u}-\mathbf{u}_h,\nabla\varphi)\\ &\leqslant C\|\mathbf{u}-\mathbf{u}_h\|h\|\varphi\|_2 + (\mathbf{u}-\mathbf{u}_h,\nabla\varphi),\end{aligned} \tag{3.17}$$

using (3.3). We manipulate the second term on the right in (3.17) in the following way:

$$\begin{aligned}(\mathbf{u}-\mathbf{u}_h,\nabla\varphi) &= \left(\nabla\cdot(\mathbf{u}-\mathbf{u}_h),\varphi-\hat{\varphi}\right)\\ &= \left(\nabla\cdot\left(\mathbf{u}-\Pi^*\mathbf{u}\right),\varphi-\hat{\varphi}\right) + \left(\nabla\cdot\left(\Pi^*\mathbf{u}-\mathbf{u}_h\right),\varphi-\hat{\varphi}\right)\\ &\leqslant C\|\mathbf{u}\|_1 h\|\varphi\|_1 + \left(\nabla\cdot\left(\Pi^*\mathbf{u}-\mathbf{u}_h\right),\varphi-\hat{\varphi}\right)_{\Omega^*},\end{aligned} \tag{3.18}$$

using (3.9), (3.7) and (3.6). To bound the last term in (3.18) we consider separately the two-dimensional and the three-dimensional cases. The reason for this is that we employ the Sobolev embedding inequality [1]

$$\|\varphi\|_{1,p} \leqslant C\|\varphi\|_2, \quad 2 \leqslant p \leqslant \frac{2d}{d-2},$$

which implies

$$\|\varphi\|_{1,\infty} \leqslant C\|\varphi\|_2, \quad d=2, \tag{3.19}$$

and

$$\|\varphi\|_{1,6} \leqslant C\|\varphi\|_2, \quad d=3. \tag{3.20}$$

If $d=2$ we write

$$\begin{aligned}\left(\nabla\cdot\left(\Pi^*\mathbf{u}-\mathbf{u}_h\right),\varphi-\hat{\varphi}\right)_{\Omega^*} &\leqslant \left\|\nabla\cdot\left(\Pi^*\mathbf{u}-\mathbf{u}_h\right)\right\|_{\Omega^*}\|\varphi-\hat{\varphi}\|_{\Omega^*}\\ &\leqslant Ch^{-1}\left\|\Pi^*\mathbf{u}-\mathbf{u}_h\right\|_{\Omega^*}h\|\varphi\|_{1,\Omega^*}\\ &\leqslant Ch^{1/2}\left(\|p\|_{1,\infty,\Omega^*}+\|\mathbf{u}\|_1\right)h^{1/2}\|\varphi\|_{1,\infty,\Omega^*}\\ &\leqslant Ch\left(\|p\|_{1,\infty,\Omega^*}+\|\mathbf{u}\|_1\right)\|\varphi\|_2,\end{aligned} \tag{3.21}$$

where we used the inverse inequality, (3.6), (3.13), the fact that $|\Omega^*| \leqslant Ch$, and (3.19). For $d=3$ we bound the above term in the following way, using Hölder's inequality:

$$\begin{aligned}\left(\nabla\cdot\left(\Pi^*\mathbf{u}-\mathbf{u}_h\right),\varphi-\hat{\varphi}\right)_{\Omega^*} &\leqslant \left\|\nabla\cdot\left(\Pi^*\mathbf{u}-\mathbf{u}_h\right)\right\|_{L^{6/5}(\Omega^*)}\|\varphi-\hat{\varphi}\|_{L^6(\Omega^*)}\\ &\leqslant C\left\|\nabla\cdot\left(\Pi^*\mathbf{u}-\mathbf{u}_h\right)\right\|_{L^{6/5}(\Omega^*)}h\|\varphi\|_{1,6,\Omega^*}\\ &\leqslant C\left\|\nabla\cdot\left(\Pi^*\mathbf{u}-\mathbf{u}_h\right)\right\|_{L^{6/5}(\Omega^*)}h\|\varphi\|_{2,\Omega^*},\end{aligned} \tag{3.22}$$

using the L^p-version of (3.6) (see [11]) and (3.20). To complete the argument we again employ Hölder's inequality. For any $1 < p < \infty$

$$\|\phi\|_{L^p(G)} \leqslant \left\{\left(\int_G \phi^2\,\mathrm{d}x\right)^{p/2}\left(\int_G 1\,\mathrm{d}x\right)^{1-p/2}\right\}^{1/p} = \|\phi\|_{L^2(G)}|G|^{(2-p)/(2p)},$$

which, with $\phi = \nabla \cdot (\Pi^* \mathbf{u} - \mathbf{u}_h)$, $G = \Omega^*$, and $p = 6/5$, implies

$$\left\| \nabla \cdot \left(\Pi^* \mathbf{u} - \mathbf{u}_h \right) \right\|_{L^{6/5}(\Omega^*)} \leqslant C \left\| \nabla \cdot \left(\Pi^* \mathbf{u} - \mathbf{u}_h \right) \right\|_{L^2(\Omega^*)} h^{1/3}.$$

Substituting this bound into (3.22) gives

$$\begin{aligned} \left(\nabla \cdot \left(\Pi^* \mathbf{u} - \mathbf{u}_h \right), \varphi - \hat{\varphi} \right)_{\Omega^*} &\leqslant C h^{-1} \left\| \Pi^* \mathbf{u} - \mathbf{u}_h \right\| h^{1/3} h \|\varphi\|_2 \\ &\leqslant C \left(\|p\|_{1,\infty,\Omega^*} + \|\mathbf{u}\|_1 \right) h^{5/6} \|\varphi\|_2, \end{aligned} \tag{3.23}$$

using (3.13). The combination of (3.15)–(3.21) and (3.23), along with (3.14) and (3.6) gives the following result.

Theorem 3.2. For the pressure p_h of the mixed method (2.6), (2.7), there exists a constant C dependent on Ω and $\|K\|_{1,\infty}$ but independent of h such that

$$\|p - p_h\| \leqslant C \left(\|p\|_{1,\infty,\Omega^*} + \|\mathbf{u}\|_{1,\Omega} \right) h^r, \tag{3.24}$$

where $r = 1$ if $d = 2$ and $r = 5/6$ if $d = 3$.

3.3. Interior velocity error estimates

We establish interior error bounds for $\mathbf{u} - \mathbf{u}_h$. Let Ω_i' be compactly contained in Ω_i, $i = 1, \ldots, n$, and let $\Omega' = \bigcup_{i=1}^n \Omega_i'$. We assume that h is small enough so that $\Omega' \cap \Omega^* = \emptyset$.

Theorem 3.3. For any $\varepsilon > 0$, there exists a constant C_ε independent of h such that

$$\|\mathbf{u} - \mathbf{u}_h\|_{\Omega'} \leqslant C_\varepsilon \left(\|p\|_{1,\infty,\Omega^*} + \|\mathbf{u}\|_{1,\Omega} \right) h^{r-\varepsilon}, \tag{3.25}$$

where $r = 1$ if $d = 2$ and $r = 5/6$ if $d = 3$.

We will need the following lemma.

Lemma 3.3. If $\phi \in C^\infty(\Omega)$ and $\mathbf{v} \in \mathbf{V}_h^*$, then there exists a constant independent of h such that

$$\left\| \left(I - \Pi^* \right)(\phi \mathbf{v}) \right\| \leqslant C \|\mathbf{v}\| \|\phi\|_1 h. \tag{3.26}$$

Proof. For any $\mathbf{v} \in \mathbf{V}_h^*$ consider the functional $l_{\mathbf{v}}(\phi) = \phi \mathbf{v} - \Pi^*(\phi \mathbf{v})$. Since $l_{\mathbf{v}}(\phi) = 0$ for all constant functions ϕ, the statement of the lemma follows from the Bramble–Hilbert lemma [11]. □

Proof of theorem 3.3. For $i = 1, \ldots, n$ and $j = 1, 2, \ldots$, fix domains Ω_i^j such that

$$\Omega_i' \subset\subset \Omega_i^{j+1} \subset\subset \Omega_i^j \subset\subset \Omega_i, \qquad \Omega^j = \bigcup_{i=1}^n \Omega_i^j,$$

and let $0 \leqslant \phi_{j+1} \in C_0^\infty(\Omega^j)$ with $\phi_{j+1} \equiv 1$ on Ω^{j+1}. We have, using (3.8) with $\mathbf{v} = \Pi^*(\phi_{j+1}(\Pi^*\mathbf{u} - \mathbf{u}_h))$ for some $c > 0$,

$$\begin{aligned} c\big\|\phi_{j+1}^{1/2}(\mathbf{u}-\mathbf{u}_h)\big\|_{\Omega^j}^2 &\leqslant \big(K^{-1}(\mathbf{u}-\mathbf{u}_h), \phi_{j+1}(\mathbf{u}-\mathbf{u}_h)\big)_{\Omega^j} \\ &= \big(K^{-1}(\mathbf{u}-\mathbf{u}_h), \phi_{j+1}\big(\mathbf{u}-\Pi^*\mathbf{u}\big)\big)_{\Omega^j} \\ &\quad + \big(K^{-1}(\mathbf{u}-\mathbf{u}_h), \big(I-\Pi^*\big)\big(\phi_{j+1}\big(\Pi^*\mathbf{u}-\mathbf{u}_h\big)\big)\big)_{\Omega^j} \\ &\quad + \big(p-p_h, \nabla\cdot\Pi^*\big(\phi_{j+1}\big(\Pi^*\mathbf{u}-\mathbf{u}_h\big)\big)\big)_{\Omega^j} \\ &\leqslant C\big\{\big\|\phi_{j+1}^{1/2}(\mathbf{u}-\mathbf{u}_h)\big\|_{\Omega^j}\big\|\mathbf{u}-\Pi^*\mathbf{u}\big\|_{\Omega^j} \\ &\qquad + \|\mathbf{u}-\mathbf{u}_h\|_{\Omega^j}\big\|\Pi^*\mathbf{u}-\mathbf{u}_h\big\|_{\Omega^j}\|\phi_{j+1}\|_{1,\Omega^j}h \\ &\qquad + \big(p-p_h, \nabla\cdot\Pi^*\big(\phi_{j+1}\big(\Pi^*\mathbf{u}-\mathbf{u}_h\big)\big)\big)_{\Omega^j}\big\}, \end{aligned} \tag{3.27}$$

where we used lemma 3.3 in the second inequality. For the last term in (3.27) we have, using that $\nabla\cdot(\Pi^*\mathbf{u}-\mathbf{u}_h) = 0$ on Ω^j,

$$\begin{aligned} \big(p-p_h, \nabla\cdot\Pi^*\big(\phi_{j+1}\big(\Pi^*\mathbf{u}-\mathbf{u}_h\big)\big)\big)_{\Omega^j} &= \big(\hat{p}-p_h, \nabla\cdot\big(\phi_{j+1}\big(\Pi^*\mathbf{u}-\mathbf{u}_h\big)\big)\big)_{\Omega^j} \\ &= \big(\hat{p}-p_h, \nabla\phi_{j+1}\cdot\big(\Pi^*\mathbf{u}-\mathbf{u}_h\big)\big)_{\Omega^j} \\ &\leqslant C\|\hat{p}-p_h\|_{\Omega^j}\big\|\phi_j^{1/2}\big(\Pi^*\mathbf{u}-\mathbf{u}_h\big)\big\|_{\Omega^{j-1}}. \end{aligned} \tag{3.28}$$

Thus, using (3.27), (3.28), (3.3), theorems 3.1 and 3.2,

$$\big\|\phi_{j+1}^{1/2}(\mathbf{u}-\mathbf{u}_h)\big\|_{\Omega^j} \leqslant C\big(\|p\|_{1,\infty,\Omega^*} + \|\mathbf{u}\|_{1,\Omega}\big)\big(h + h^{r/2}\big\|\phi_j^{1/2}(\mathbf{u}-\mathbf{u}_h)\big\|_{\Omega^{j-1}}^{1/2}\big). \tag{3.29}$$

Since theorem 3.1 gives

$$\big\|\phi_j^{1/2}(\mathbf{u}-\mathbf{u}_h)\big\|_{\Omega^{j-1}} \leqslant C_j h^{r/2+1/4},$$

applying (3.29) recurrently, we obtain the statement of the theorem. □

Remark 3.1. Theorems 3.2 and 3.3 imply optimal (for $d = 2$) and almost optimal (for $d = 3$) convergence for the pressure and the interior velocity, respectively.

4. Extension to two-phase flow

The method from the previous section can be extended to two-phase and three-phase (Black Oil) flow models. We present here the formulation for two-phase incompressible flow of oil and water. The governing mass conservation equations [10] are

$$\frac{\partial(\phi\rho_\alpha S_\alpha)}{\partial t} + \nabla\cdot\mathbf{U}_\alpha = q_\alpha, \tag{4.1}$$

where α = w (water), o (oil) denotes the phase, S_α is the phase saturation, $\rho_\alpha = \rho_\alpha(P_\alpha)$ is the phase density, ϕ is the porosity, q_α is the source term, and

$$\mathbf{U}_\alpha = -\frac{k_\alpha(S_\alpha)K}{\mu_\alpha}\rho_\alpha(\nabla P_\alpha - \rho_\alpha g\nabla D) \tag{4.2}$$

is the Darcy velocity. Here P_α is the phase pressure, $k_\alpha(S_\alpha)$ is the phase relative permeability, μ_α is the phase viscosity, K is the rock permeability tensor, g is the gravitational constant, and D is the depth. The above equations are coupled via the volume balance equation and the capillary pressure relation

$$S_{\mathrm{w}} + S_{\mathrm{o}} = 1, \qquad p_{\mathrm{c}}(S_{\mathrm{w}}) = P_{\mathrm{o}} - P_{\mathrm{w}}. \tag{4.3}$$

We assume for simplicity that oil and water pressures are specified on $\partial\Omega$, although more general types of boundary conditions can also be treated.

We employ a variant of the mixed finite element method, the expanded mixed method. It has been developed for accurate and efficient treatment of irregular domains (see [3,4] for single block and [25] for multiblock domains). In the context of multiphase flow this method allows for proper treatment of the degeneracies in the diffusion term (see remark 4.1).

Following [4], let, for $\alpha = \mathrm{w}, \mathrm{o}$,

$$\widetilde{\mathbf{U}}_\alpha = -\nabla P_\alpha.$$

Then

$$\mathbf{U}_\alpha = \frac{k_\alpha(S_\alpha)K}{\mu_\alpha}\rho_\alpha\big(\widetilde{\mathbf{U}}_\alpha + \rho_\alpha g \nabla D\big).$$

Let $0 = t_0 < t_1 < t_2 < \cdots$, let $\Delta t^n = t_n - t_{n-1}$, and let $f^n = f(t_n)$. In the backward Euler expanded mixed finite element approximation of (4.1)–(4.3) we seek, for $n = 1, 2, 3, \ldots$, $\mathbf{U}^n_{h,\alpha} \in \mathbf{V}_h$, $\widetilde{\mathbf{U}}^n_{h,\alpha} \in \mathbf{V}_h$, $P^n_{h,\alpha} \in W_h$, and $S^n_{h,\alpha} \in W_h$ such that, for $\alpha = \mathrm{o}$ and w,

$$\int_\Omega \frac{(\phi\rho_{h,\alpha}S_{h,\alpha})^n - (\phi\rho_{h,\alpha}S_{h,\alpha})^{n-1}}{\Delta t^n} w \,\mathrm{d}x + \int_\Omega \nabla\cdot\mathbf{U}^n_{h,\alpha} w \,\mathrm{d}x = \int_\Omega q_\alpha w \,\mathrm{d}x, \qquad w \in W_h, \tag{4.4}$$

$$\int_\Omega \widetilde{\mathbf{U}}^n_{h,\alpha}\cdot\mathbf{v}\,\mathrm{d}x = \int_\Omega P^n_{h,\alpha}\nabla\cdot\mathbf{v}\,\mathrm{d}x - \int_{\partial\Omega} P^n_{h,\alpha}\mathbf{v}\cdot\nu_k\,\mathrm{d}\sigma, \qquad \mathbf{v}\in\mathbf{V}_h, \tag{4.5}$$

$$\int_{\Omega_k} \mathbf{U}^n_{h,\alpha}\cdot\tilde{\mathbf{v}}\,\mathrm{d}x = \int_\Omega \frac{k^n_{h,\alpha}K}{\mu_{h,\alpha}}\rho^n_{h,\alpha}\big(\widetilde{\mathbf{U}}^n_{h,\alpha} + \rho^n_{h,\alpha}g\nabla D\big)\cdot\tilde{\mathbf{v}}\,\mathrm{d}x, \quad \tilde{\mathbf{v}}\in\mathbf{V}_h. \tag{4.6}$$

Remark 4.1. Introducing the pressure gradients $\widetilde{\mathbf{U}}_\alpha$ in the expanded mixed method allows for proper handling of the degenerate (for $S_\alpha = 0$) relative permeability $k_\alpha(S_\alpha)$ in (4.5), (4.6). It also allows, even for a full permeability tensor K, to accurately approximate the mixed method on each subdomain by cell-centered finite differences for P_{o} and S_{o}. This is achieved by approximating the vector integrals in (4.5) and (4.6) by a trapezoidal quadrature rule and eliminating $\widetilde{\mathbf{U}}_{h,\alpha}$ and $\mathbf{U}_{h,\alpha}$ from the system [3,4].

5. Numerical experiments

5.1. Implementation

We briefly discuss the implementation of the enhanced velocity method in IPARS. For simplicity we concentrate on the single-phase system (2.6), (2.7) with a diagonal permeability tensor K. As we mentioned above, the mixed finite element method is reduced to cell-centered finite differences for the pressure. An application of the trapezoidal quadrature rule to the integral $(K^{-1}\mathbf{u}, \mathbf{v})$ in (2.6) allows to express, on any edge (face) away from the interface, the normal velocity as a transmissibility coefficient times the difference of the pressures in the neighboring cells (see [20] for details). To describe the equations on the interface, let us consider figure 3. Assume that the permeability in the direction orthogonal to the interface has values K_a, K_{b_1}, and K_{b_2} on elements a, b_1, and b_2, respectively. Using the trapezoidal rule approximation of (2.6), the flux q_i on e_i is given by

$$q_i = -T_i(p_a - p_{b_i}), \quad i = 1, 2, \tag{5.1}$$

where

$$T_i = 2|e_i|\left(\frac{h_a}{K_a} + \frac{h_b}{K_{b_i}}\right)$$

is the transmissibility coefficient on e_i. The flux q on $e = e_1 \cup e_2$ is given by

$$q = q_1 + q_2. \tag{5.2}$$

The mass conservation (2.7) for element a couples, via (5.1), p_a with p_{b_1} and p_{b_2}. This coupling introduces irregularity in the data structure for the algebraic system. To avoid this difficulty, a ghost layer around the boundary of each subdomain is utilized, see figure 4. Note the ghost layer is also used for communication between processors on multiprocessor machines. A new pressure variable p_a^e is introduced in the ghost cell. The flux q can then be written as

$$q = -T\left(p_a - p_a^e\right), \tag{5.3}$$

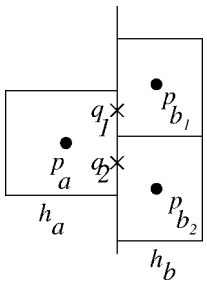

Figure 3. Finite differences on the interface.

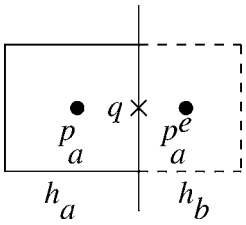

Figure 4. Ghost cell pressure.

where $T = T_1 + T_2$. Equations (5.1)–(5.3) can be used to solve for p_a^e in terms of p_{b_1} and p_{b_2}. In our case we obtain

$$p_a^e = \frac{T_1 p_{b_1} + T_2 p_{b_2}}{T}.$$

A Krylov space iterative solver is employed in IPARS for solving the algebraic system. In the case of multiphase flow, Newton's method is applied for the nonlinear system, and GMRES is used for solving the Jacobian system. The iterative solver only requires matrix–vector products. The above change of variables allows for preserving the regular structure of the algebraic system. We should also point out that the IPARS implementation exhibits very good parallel scalability, although such studies are not presented here.

5.2. *Single-phase flow*

In this section we present two numerical studies for single-phase flow confirming the theory of section 3. Both examples are set on $\Omega = (0, 6) \times (0, 6) \subset \mathbb{R}^2$ and employ Dirichlet boundary conditions. The domain is divided into four subdomains with interfaces along the lines $x = 3$ and $y = 3$. The initial non-matching subdomain grids are 4×4, 5×6, 5×3, and 4×4. The rates were established by running the test cases and 4 levels of grid refinement, each time halving the element diameters.

The first problem we consider has a smooth solution

$$p(x, y) = x^3 y^4 + x^2 + \sin(xy)\cos(y)$$

and permeability coefficient

$$K = \begin{pmatrix} (x+1)^2 + y^2 & 0 \\ 0 & (x+1)^2 \end{pmatrix}.$$

The convergence results are given in table 1. The pressure error $|||p - p_h|||$ is the discrete L^2-norm induced by the midpoint rule on $\mathcal{T}_h$. The discrete L^2 velocity error $|||\mathbf{u} - \mathbf{u}_h|||$ is based on the values of the normal component at the midpoint of the edges. The interior velocity error $|||\mathbf{u} - \mathbf{u}_h|||_{\Omega'}$ is computed on a fixed domain Ω' which does not include one interface cell layer at the first refinement level. The numerically observed convergence rates correspond to those predicted by the theory. The pressure and velocity computed by the enhanced velocity scheme on the first level of refinement are shown in figure 5.

Table 1
Discrete norm errors and convergence rates for example 1.

Level	$\|\|\|p - p_h\|\|\|$	$\|\|\|\mathbf{u} - \mathbf{u}_h\|\|\|$	$\|\|\|\mathbf{u} - \mathbf{u}_h\|\|\|_{\Omega'}$
0	3.26E−02	3.33E−02	2.17E−02
1	8.83E−03	1.38E−02	8.88E−03
2	3.67E−03	7.87E−03	3.81E−03
3	1.87E−03	5.11E−03	1.52E−03
4	9.68E−04	3.49E−03	7.23E−04
Rate	$O(h^{0.95})$	$O(h^{0.55})$	$O(h^{1.07})$

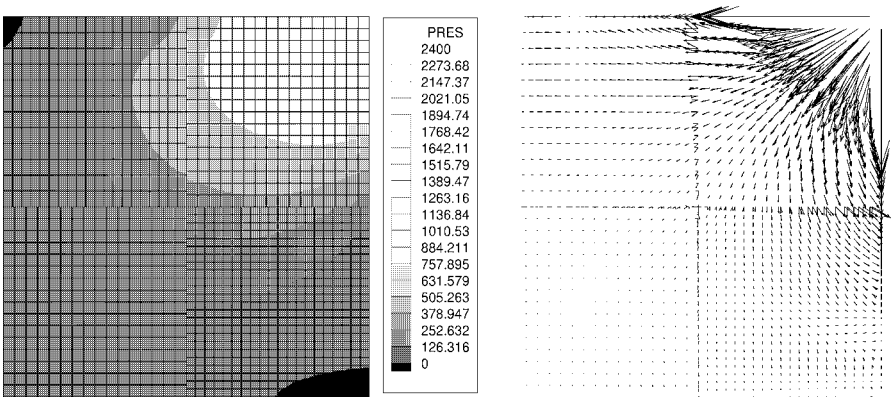

Figure 5. Computed pressure (shade) and velocity (arrows) for example 1.

In the second example we test a problem with a discontinuous coefficient. The permeability is a piecewise constant function

$$K = \begin{cases} 1, & x < 3 \text{ and } y < 3, \\ 100, & x > 3 \text{ and } y > 3, \\ 10, & \text{otherwise}, \end{cases}$$

and the true pressure solution is

$$p(x, y) = \frac{1}{K}(x - 3)(y - 3)\sin(xy).$$

Note that the pressure is continuous, although not continuously differentiable, and the normal velocity component is also continuous across the interface. As it can be seen in table 2, all three errors exhibit super-convergence of second order. The reason for the higher order is that the tangential velocity component is zero on the interface and the effect of the non-matching grids is small. This is also confirmed by the fact that the full domain and the interior velocity errors are very close. A plot of the computed solution is given in figure 6.

Table 2
Discrete norm errors and convergence rates for example 2.

Level	$\|\|\| p - p_h \|\|\|$	$\|\|\| \mathbf{u} - \mathbf{u}_h \|\|\|$	$\|\|\| \mathbf{u} - \mathbf{u}_h \|\|\|_{\Omega'}$
0	2.74E−01	4.31E−01	4.31E−01
1	5.65E−02	1.34E−01	1.35E−01
2	1.37E−02	3.76E−02	3.28E−02
3	3.40E−03	9.71E−03	8.05E−03
4	8.47E−04	2.47E−03	1.99E−03
Rate	$O(h^{2.01})$	$O(h^{1.97})$	$O(h^{2.02})$

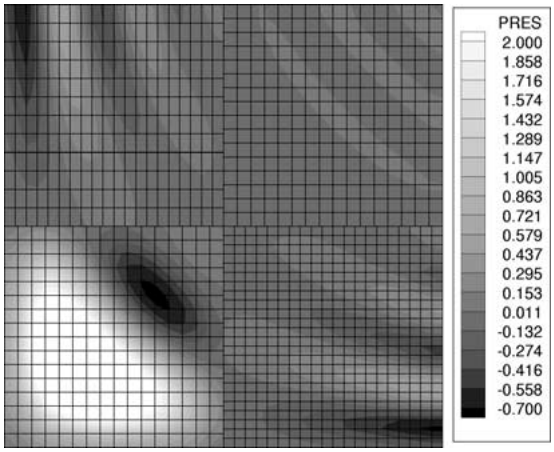

Figure 6. Computed pressure for example 2.

5.3. *Two-phase flow*

Here we test the enhanced velocity scheme for modeling two-phase incompressible flow in porous media and compare its behavior to that of the mortar method. We model oil–water displacement in a heterogeneous reservoir. The domain is a square with dimensions 420×420 ft divided into 4 subdomains. The computational grids are 42×42 and 35×30 in a checkerboard fashion. In the mortar run the mortar space is discontinuous piecewise linear and the mortar grid on each interface has 21 elements with 42 degrees of freedom. The grids and the permeability field (which varies three orders of magnitude) are given in figure 7. Initially oil pressure is 500 psi and water saturation is 0.22. Water is injected at the lower left corner. A production well is placed at the upper right corner. Water saturation profiles for both methods after 2651 days of injection are given in figure 8. The plots indicate that the two schemes produce very similar solutions. This is also confirmed by the production well rates and oil–water ratios plotted in figure 9. The closeness of these results may seem surprising at first due to the different convergence properties of the two methods. We believe the reason for this is that the

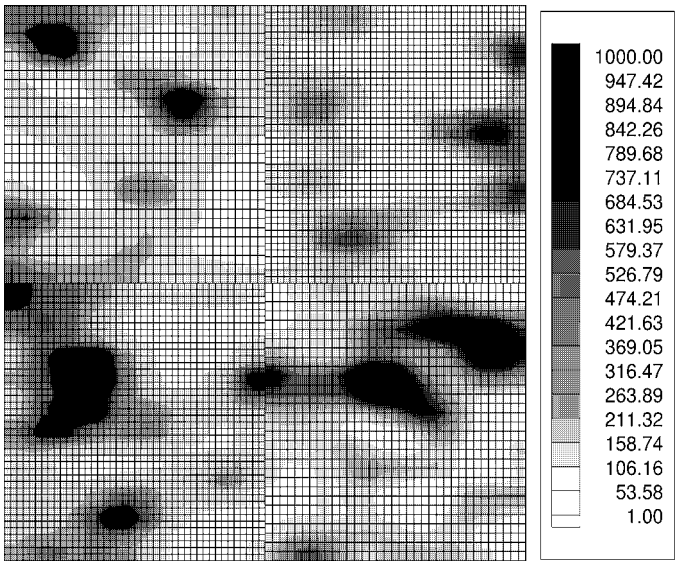

Figure 7. Permeability field and computational grids in the two-phase example.

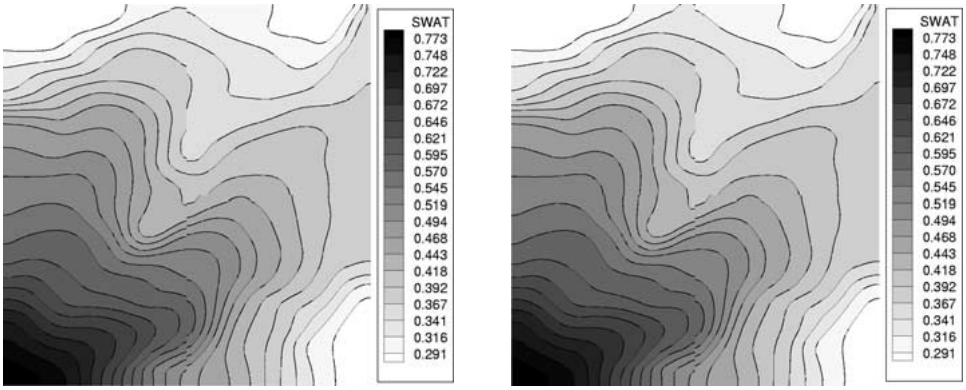

A. *Enhanced velocity* B. *Discontinuous mortars*

Figure 8. Water saturation profiles after 2651 days of injection.

dominant source of error in this case are the wells, not the non-matching grids. However, there is a big difference in the efficiency of the two methods. For this test case the enhanced velocity scheme is approximately 8 times faster than the mortar scheme. This is expected, since the former scheme avoids the solution of an interface problem and its computational cost is comparable to solving a single-block problem. In fairness we should mention that in the current mortar implementation a nonlinear interface problem is being solved. Although very flexible and suitable for multiphysics applications, this formulation is somewhat slow. A better mortar solver is being implemented.

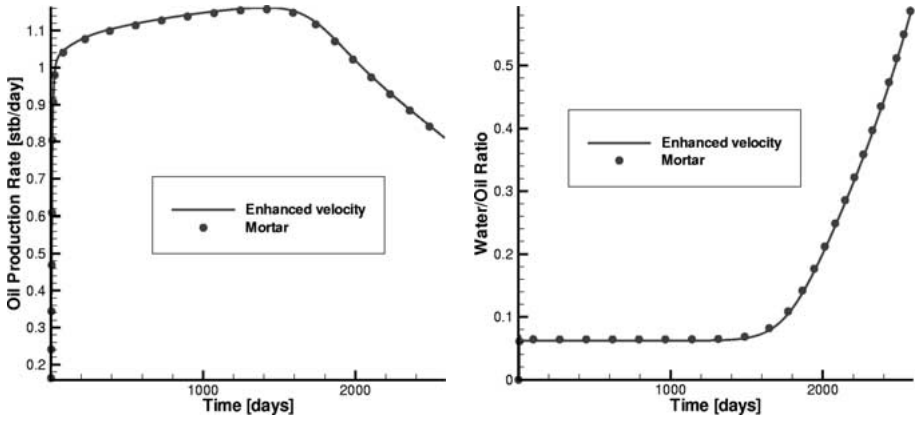

A. *Oil production rate* B. *Water/oil ratio*

Figure 9. Well rates.

6. Conclusions

A new approach to modeling flow in porous media via mixed finite element methods on non-matching multiblock grids is presented. The method is somewhat simpler and less expensive than the mortar method, since flux continuity is incorporated in the velocity space. Theoretical a priori estimates and numerical studies for single-phase flow show almost optimal convergence for pressure and interior velocity. Computational results for two-phase flow indicate that the enhanced velocity method provides accuracy comparable to the mortar method at substantially reduced cost.

Acknowledgements

The authors would like to acknowledge the contributions of Malgorzata Peszynska, Qin Lu, and Manish Parashar to the development of IPARS.

Mary F. Wheeler is partially supported by the DOE grant DE-FG03-99ER25371, and the NSF grant DMS 9873326. Ivan Yotov is partially supported by the DOE grant DE-FG03-99ER25371, the NSF grants DMS 9873326 and DMS 0107389, and the University of Pittsburgh CRDF grant.

References

[1] R.A. Adams, *Sobolev Spaces*, Pure and Applied Mathematics, Vol. 65 (Academic Press, New York/London, 1975).

[2] T. Arbogast, L.C. Cowsar, M.F. Wheeler and I. Yotov, Mixed finite element methods on non-matching multiblock grids, SIAM J. Numer. Anal. 37 (2000) 1295–1315.

[3] T. Arbogast, C.N. Dawson, P.T. Keenan, M.F. Wheeler and I. Yotov, Enhanced cell-centered finite differences for elliptic equations on general geometry, SIAM J. Sci. Comput. 19(2) (1998) 404–425.

[4] T. Arbogast, M.F. Wheeler and I. Yotov, Mixed finite elements for elliptic problems with tensor coeffcients as cell-centered finite differences, SIAM J. Numer. Anal. 34(2) (1997) 828–852.

[5] T. Arbogast and I. Yotov, A non-mortar mixed finite element method for elliptic problems on non-matching multiblock grids, Comput. Methods Appl. Mech. Engrg. 149 (1997) 255–265.
[6] F. Ben Belgacem, The mortar finite element method with Lagrange multipliers, Numer. Math. 84(2) (1999) 173–197.
[7] F. Ben Belgacem, The mixed mortar finite element method for the incompressible Stokes problem: Convergence analysis, SIAM J. Numer. Anal. 37(4) (2000) 1085–1100.
[8] C. Bernardi, Y. Maday and A.T. Patera, A new nonconforming approach to domain decomposition: the mortar element method, in: *Nonlinear Partial Differential Equations and Their Applications*, eds. H. Brezis and J.L. Lions (Longman Scientific & Technical, UK, 1994).
[9] F. Brezzi and M. Fortin, *Mixed and Hybrid Finite Element Methods* (Springer, New York, 1991).
[10] G. Chavent and J. Jaffre, *Mathematical Models and Finite Elements for Reservoir Simulation* (North-Holland, Amsterdam, 1986).
[11] P.G. Ciarlet, *The Finite Element Method for Elliptic Problems* (North-Holland, New York, 1978).
[12] M.G. Edwards, Elimination of adaptive grid interface errors in the discrete cell centered pressure equation, J. Comput. Phys. 126 (1996) 356–372.
[13] R. Ewing, R. Lazarov, T. Lin and Y. Lin, Mortar finite volume element approximations of second order elliptic problems, East-West J. Numer. Math. 8(2) (2000) 93–110.
[14] R.E. Ewing, R.D. Lazarov and P.S. Vassilevski, Local refinement techniques for elliptic problems on cell-centered grids. I. Error analysis, Math. Comp. 56(194) (1991) 437–461.
[15] V. Girault and P.A. Raviart, *Finite Element Methods for Navier–Stokes Equations. Theory and Algorithms* (Springer, Berlin, 1986).
[16] P. Grisvard, *Elliptic Problems in Nonsmooth Domains* (Pitman, Boston, 1985).
[17] J.C. Nedelec, Mixed finite elements in $\mathbb{R}^3$, Numer. Math. 35 (1980) 315–341.
[18] R.A. Raviart and J.M. Thomas, A mixed finite element method for 2nd order elliptic problems, in: *Mathematical Aspects of the Finite Element Method*, Lecture Notes in Mathematics, Vol. 606 (Springer, New York, 1977) pp. 292–315.
[19] J.E. Roberts and J.-M. Thomas, Mixed and hybrid methods, in: *Handbook of Numerical Analysis*, eds. P.G. Ciarlet and J.L. Lions, Vol. II (Elsevier Science, Amsterdam, 1991) pp. 523–639.
[20] T.F. Russell and M.F. Wheeler, Finite element and finite difference methods for continuous flows in porous media, in: *The Mathematics of Reservoir Simulation*, ed. R.E. Ewing (SIAM, Philadelphia, PA, 1983) pp. 35–106.
[21] J.M. Thomas, These de Doctorat d'état, l'Université Pierre et Marie Curie (1977).
[22] M.F. Wheeler, T. Arbogast, S. Bryant, J. Eaton, Q. Lu, M. Peszynska and I. Yotov, A parallel multiblock/multidomain approach to reservoir simulation, in: *Fifteenth SPE Symposium on Reservoir Simulation*, SPE 51884, Houston, TX, Society of Petroleum Engineers, 1999, pp. 51–62.
[23] M.F. Wheeler, J.A. Wheeler and M. Peszynska, A distributed computing portal for coupling multiphysics and multiple domains in porous media, in: *Computational Methods in Water Resources*, eds. L.R. Bentley, J.F. Sykes, C.A. Brebbia, W.G. Gray and G.F. Pinder (A.A. Balkema, 2000) pp. 167–174.
[24] B.I. Wohlmuth, A mortar finite element method using dual spaces for the Lagrange multiplier, SIAM J. Numer. Anal. 38(3) (2000) 989–1012.
[25] I. Yotov, Mixed finite element methods for flow in porous media, Ph.D. thesis, Rice University, Houston, TX (1996); also TR96-09, Dept. Comp. Appl. Math., Rice University and TICAM Report 96-23, University of Texas at Austin.